

Fast spinning strange stars: possible ways to constrain interacting quark matter parameters

Sudip Bhattacharyya^{1*}, Ignazio Bombaci^{2,3,4}, Domenico Logoteta³, Arun V. Thampan^{5,6}

¹*Department of Astronomy and Astrophysics, Tata Institute of Fundamental Research, Mumbai 400005, India*

²*Dipartimento di Fisica, Università di Pisa, Largo B. Pontecorvo, 3 I-56127 Pisa, Italy*

³*INFN, Sezione di Pisa, Largo B. Pontecorvo, 3 I-56127 Pisa, Italy*

⁴*European Gravitational Observatory, Via E. Amaldi, I-56021 S. Stefano a Macerata, Cascina Italy*

⁵*Department of Physics, St. Joseph's College, 36 Lalbagh Road, Bangalore 560027, India*

⁶*Inter-University Centre for Astronomy and Astrophysics (IUCAA), India*

Accepted XXX. Received YYY; in original form ZZZ

ABSTRACT

For a set of equation of state (EoS) models involving interacting strange quark matter, characterized by an effective bag constant (B_{eff}) and a perturbative QCD corrections term (a_4), we construct fully general relativistic equilibrium sequences of rapidly spinning strange stars for the first time. Computation of such sequences is important to study millisecond pulsars and other fast spinning compact stars. Our EoS models can support a gravitational mass (M_G) and a spin frequency (ν) at least up to $\approx 3.0M_\odot$ and ≈ 1250 Hz respectively, and hence are fully consistent with measured M_G and ν values. This paper reports the effects of B_{eff} and a_4 on measurable compact star properties, which could be useful to find possible ways to constrain these fundamental quark matter parameters, within the ambit of our EoS models. We confirm that a lower B_{eff} allows a higher mass. Besides, for known M_G and ν , measurable parameters, such as stellar radius, radius-to-mass ratio and moment of inertia, increase with the decrease of B_{eff} . Our calculations also show that a_4 significantly affects the stellar rest mass and the total stellar binding energy. As a result, a_4 can have signatures in evolutions of both accreting and non-accreting compact stars, and the observed distribution of stellar mass and spin and other source parameters. Finally, we compute the parameter values of two important pulsars, PSR J1614-2230 and PSR J1748-2446ad, which may have implications to probe their evolutionary histories, and for constraining EoS models.

Key words: equation of state – methods: numerical – pulsars: individual: PSR J1614-2230, PSR J1748-2446ad – relativity – stars: neutron – stars: rotation

1 INTRODUCTION

Despite more than 80 years since the proposal of neutron stars as a new class of astrophysical objects (Baade & Zwicky 1934) and about 50 years since their first discovery as radio pulsars (Hewish et al. 1968), their true nature and internal composition still remain one of the most fascinating enigma in modern astrophysics.

The bulk properties and the internal constitution of compact stars (neutron stars) primarily depend on the equation of state (EoS) of strong interacting matter, i.e. on the thermodynamical relation between the matter pressure, energy density and temperature. Determining the correct EoS model describing the interior of compact stars is a funda-

mental problem of physics, and a major effort has been made during the last few decades to solve this problem by measuring the stellar bulk properties. A number of these measurement methods for low-mass X-ray binaries (LMXBs), based on thermonuclear X-ray bursts, regular X-ray pulsations, high-frequency quasi-periodic oscillations, broad relativistic spectral emission lines, quiescent emissions and orbital motions, have been reviewed in Bhattacharyya (2010). Spectral and timing properties of non-accreting millisecond radio pulsars can also be useful to measure stellar mass and radius (e.g., Bogdanov & Grindlay (2009); Bogdanov et al. (2008)). However, until recently theoretically proposed EoS models could not be effectively constrained because of systematic uncertainties (e.g., Bhattacharyya (2010)).

The recent precise measurement of the mass ($1.97 \pm 0.04M_\odot$) of the millisecond pulsar PSR J1614-2230 has ruled

* E-mail: sudip@tifr.res.in

out all EoS models which cannot support such high values of masses (Demorest et al. 2010). However, in response to this discovery, new realistic EoS models, that support high mass, have been proposed. So essentially all types of EoS models, such as nucleonic, hyperonic, strange quark matter, hybrid, still survive, and it is still a very important problem to constrain compact star EoS models.

In this paper, we are interested in fast spinning compact stars. So far the spin frequencies of a number of such stars have been measured (e.g., Watts (2012); Patruno & Watts (2012); Smedley et al. (2014)). Some of these sources are binary millisecond radio pulsars, and the masses of a fraction of them have been relatively precisely measured (e.g., Smedley et al. (2014)). In order to constrain EoS models, three independent bulk parameters of a given compact star are to be measured, and the third observable parameter (after the mass and spin) could be the stellar radius (Lo et al. 2013; Bogdanov & Grindlay 2009) or the moment of inertia (Morrison et al. 2004). Here we note that a very high observed spin frequency could constrain EoS models, but so far the highest spin frequency observed is 716 Hz from a radio pulsar PSR J1748-2446ad (Hessels et al. 2006). This spin frequency is allowed by almost all proposed EoS models, and hence this spin measurement alone is not a useful property to constrain these models.

From a fundamental point of view, the EoS of strongly interacting matter should be derived by numerically solving quantum chromodynamics (QCD) equations on a space-time lattice (lattice QCD). Since the central density of compact stars can significantly exceed the saturation density ($\sim 2.8 \times 10^{14}$ g/cm³) of nuclear matter and their temperature could be considered equal to zero after a few minutes of their formation (Burrows & Lattimer 1986; Bombaci et al. 1995; Prakash et al. 1997), these compact stars can be viewed as natural laboratories to explore the phase diagram of QCD in the low temperature T and high baryon chemical potential μ_b region. In this region of the QCD phase diagram a transition to a phase with deconfined quarks and gluons is expected to occur and to influence a number of interesting astrophysical phenomena (Perez-Garcia et al. 2010; Sotani et al. 2011; Berezhiani et al. 2003; Bombaci et al. 2007, 2011; Weissenborn et al. 2011; Nishimura et al. 2012).

Recent high precision lattice QCD calculations at zero baryon chemical potential (i.e. zero baryon density) have clearly shown that at high temperature and for physical values of the quark masses, quarks and gluons become the most relevant degrees of freedom. The transition to this quark gluon plasma phase is a crossover (Bernard et al. 2005; Cheng et al. 2006; Aoki et al. 2006) rather than a real phase transition. Lattice QCD calculations in this regime have also distinctly demonstrated the importance of taking into account the interactions of quarks and gluons since the calculated EoS significantly deviates from that of an ideal gas.

Unfortunately, current lattice QCD calculations at finite baryon chemical potential are plagued with the so called “sign problem”, which makes them unrealizable by all known lattice methods. Thus, to explore the QCD phase diagram at low temperature T and high μ_b , it is necessary to invoke some approximations in QCD or to apply some QCD effective model.

Along these lines, for example, a model of the equation of state (EoS) of strange quark matter (SQM) (Farhi & Jaffe 1984) inspired by the MIT bag model of hadrons (Chodos et al. 1974) has been extensively used by many authors to calculate the structure of strange stars (Witten 1984; Alcock et al. 1986; Haensel et al. 1986; Li et al. 1999a,b; Xu et al. 1999), or the structure of the so called hybrid stars, *i.e.* compact stars with an SQM core. In this model SQM is treated as an ideal relativistic Fermi gas of *up* (u), *down* (d) and *strange* (s) quarks (together with an appropriate number of electrons to guarantee electric charge neutrality and equilibrium with respect to the weak interactions), that reside in a region characterized by a constant energy density B . The parameter B takes into account, in a crude phenomenological manner, the nonperturbative aspects of QCD and is related to the bag constant which in the MIT bag model (Chodos et al. 1974) gives the confinement of quarks within hadrons.

The deconfinement phase transition has been also described using an EoS of quark gluon plasma derived within the Field Correlator Method (FCM) (Dosh 1987; Dosh & Simonov 1988; Simonov 1988; Di Giacomo et al. 2002) extended to finite baryon chemical potential (Simonov & Trusov 2007a,b; Simonov 2005, 2008; Nefediev et al. 2009). FCM is a nonperturbative approach to QCD which includes from first principles, the dynamics of confinement. The model is parametrized in terms of the gluon condensate G_2 and the large distance static quark-antiquark ($Q\bar{Q}$) potential V_1 . These two quantities control the EoS of the deconfined phase at fixed quark masses and temperature. The main constructive characteristic of FCM is the possibility to describe the whole QCD phase diagram as it can span from high temperature and low baryon chemical potential, to low T and high μ_b limit.

Recently, Bombaci & Logoteta (2013) have established that the values of gluon condensate G_2 extracted from the measured mass $M = 1.97 \pm 0.04 M_\odot$ of PSR J1614-2230 (Demorest et al. 2010) are fully consistent with the values of the same quantity derived within FCM, from lattice QCD calculations of the deconfinement transition temperature at zero baryon chemical potential (Borsanyi et al. 2010; Bazavov et al. 2012). FCM thus provides a powerful tool to link numerical calculations of QCD on a space-time lattice with measured compact star masses (Logoteta & Bombaci 2013).

In this paper we make use of a more traditional approach to compute the EoS of SQM. In fact, the simple version of the MIT bag model EoS can be extended to include perturbative corrections due to quark interactions, up to the second order ($\mathcal{O}(\alpha_s^2)$) in the strong structure constant α_s (Freedman & McLerran 1977, 1978; Baluni 1978; Fraga et al. 2001; Kurkela et al. 2010)¹. Within this modified bag model one can thus evaluate the non-ideal behaviour of the EoS of cold SQM at high density.

The modified bag model EoS has already been used to calculate the structure of non-spinning strange stars (Fraga et al. 2001; Alford et al. 2005; Weissenborn et al.

¹ In Farhi & Jaffe (1984) the EoS for strange quark matter was calculated up to the order $\mathcal{O}(\alpha_s)$.

2011; Fraga et al. 2014) and hybrid stars (Alford et al. 2005; Weissenborn et al. 2011).

As already mentioned, there are two types of compact stars containing SQM. The first type is represented by the so called hybrid stars, i.e. compact stars containing a quark-hadron mixed core and eventually a pure SQM inner core. The second type, strange stars, is realized when SQM satisfies the Bodmer–Witten hypothesis (Bodmer 1971; Witten 1984). According to this hypothesis SQM is absolutely stable, in other words, its energy per baryon $(E/A)_{uds}$ is less than that of the most bound atomic nuclei (^{56}Fe , ^{58}Fe , ^{62}Ni) which is ~ 930.4 MeV. The absolute stability of SQM does not preclude the existence of “ordinary” matter (Bodmer 1971; Witten 1984). In fact, under this hypothesis, atomic nuclei can be considered as metastable states (with respect to the decay to SQM droplets) having a mean-life time which is many orders of magnitude larger than the age of the Universe.

In the last few decades, many researchers (see e.g. Xu et al. (2001); Weber (2005) and references therein) have tried to identify possible clear observational signatures to distinguish whether a compact star is a strange star, a hybrid star or a “normal” neutron star (nucleonic star).

The mass-radius (M-R) relation is one of the most promising compact star features to solve this puzzle. In fact, “low mass” (i.e. $M \lesssim 1 M_{\odot}$) strange stars have $M \sim R^3$, whereas normal neutron stars, in the mass range between $0.5 M_{\odot}$ and $\sim 0.7 M_{max}$ (where M_{max} is the stellar sequence maximum mass), have a radius which is almost independent on the mass (Lattimer & Prakash 2001; Bombaci 2007). This qualitative difference in the M-R relation is due to the fact that strange stars are self-bound objects whereas normal neutron stars are bound by gravity. Constraints for the M-R relation, extracted from observational data of compact stars in the X-ray sources SAX J1808.4-3658 (Li et al. 1999a) and 4U 1728-34 (Li et al. 1999b) seem to indicate that these objects could be accreting strange stars. Note that the observations of thermonuclear X-ray bursts, which are believed to originate from unstable thermonuclear burning of accumulated accreted matter on the compact star surface, cannot preclude these LMXBs from having strange stars. This is because, according to a proposed model (Stejner & Madsen 2006), the bursts could happen on a thin crust of “ordinary” matter (i.e. a solid layer consisting of a Coulomb lattice of atomic nuclei in β -equilibrium with a relativistic electron gas, similar to the outer crust of a neutron star) separated from the main body of the strange star by a strong Coulomb barrier (Alcok et al. 1986; Stejner & Madsen 2005).

Other significant observational informations on the constitution of compact stars may come out in the next few years from the expected detection of gravitational waves from compact stars with ground-based interferometers, such as Advanced VIRGO and Advanced LIGO. In fact, it has been shown by different research groups, e.g. (Andersson et al. 2002; Benhar et al. 2007; Fu et al. 2008; Andersson et al. 2011; Rupak et al. 2013), that gravitational waves driven by r-mode instabilities or from f-, p- and g-mode oscillations could be able to discriminate among different types of compact stars.

Another interesting possibility is that both “normal” neutron stars (nucleonic stars) and quark stars (i.e. strange stars or hybrid stars) could exist in nature

(Berezhiani et al. 2002, 2003; Bombaci et al. 2004). In this scenario quark stars could be formed via a conversion process of metastable normal neutron stars (Bombaci & Datta 2000; Berezhiani et al. 2002, 2003).

Several experimental searches for strangelets (small lumps of absolutely stable SQM) have been undertaken using different techniques. For example the Alpha Magnetic Spectrometer (AMS-02) (Tomasetti 2015), on board of the International Space Station since May 2011, could be able to detect strangelets in cosmic rays with excellent charge resolution up to an atomic number $Z \sim 26$. Strangelets search in lunar soil, brought back by the NASA Apollo 11 mission, have been performed using the tandem accelerator at the Wright Nuclear Structure Laboratory at Yale (Han et al. 2009).

It is important to emphasize that all the present observational data and our present experimental and theoretical knowledge of the properties of dense matter, do not allow us to accept or to exclude the validity of the Bodmer–Witten hypothesis.

In this paper, we assume the validity of the Bodmer–Witten hypothesis and we compute equilibrium sequences of rapidly spinning strange stars in general relativity. In § 2, we describe the modified bag model EoS (Fraga et al. 2001; Alford et al. 2005; Weissenborn et al. 2011) for SQM used in our calculations and the two parameters, effective bag constant (B_{eff}) and perturbative QCD corrections term parameter (a_4), which characterize this model. In § 3, we discuss the method to compute parameters of fast spinning compact stars in stable configurations. Here we also describe various limit sequences. In § 4, we present the numbers from our numerical calculations using tables and figures. In § 5, we discuss the implications of our results, especially for constraining B_{eff} and a_4 using observations. In § 6, we summarize the key points of this paper.

2 THE MODIFIED BAG MODEL EQUATION OF STATE FOR STRANGE QUARK MATTER

The EoS for strange quark matter including the effects of gluon mediated QCD interactions between quarks up to $\mathcal{O}(\alpha_s^2)$ can be written in a straightforward and easy-to-use form similar to the simple and popular version of the MIT bag model EoS. The grand canonical potential per unit volume takes the form (we use units where $\hbar = 1$, and $c = 1$)

$$\Omega = \sum_{i=u,d,s,e} \Omega_i^0 + \frac{3}{4\pi^2} (1 - a_4) \left(\frac{\mu_b}{3} \right)^4 + B_{\text{eff}}. \quad (1)$$

where Ω_i^0 is the grand canonical potential for u , d , s quarks and electrons described as ideal relativistic Fermi gases. We take $m_u = m_d = 0$, $m_s = 100$ MeV and $m_e = 0$. The second term on the right hand side of Eq.(1) accounts for the perturbative QCD corrections to $\mathcal{O}(\alpha_s^2)$ (Fraga et al. 2001; Alford et al. 2005; Weissenborn et al. 2011) and its value represents the degree of deviations from an ideal relativistic Fermi gas EoS, with $a_4 = 1$ corresponding to the ideal gas. The baryon chemical potential μ_b can be written in terms of the u , d and s quark chemical potentials as $\mu_b = \mu_u + \mu_d + \mu_s$. The term B_{eff} is an effective bag constant which takes

into accounts in a phenomenological way of nonperturbative aspects of QCD.

Using standard thermodynamical relations, the energy density can be written as:

$$\varepsilon = \sum_{i=u,d,s,e} \Omega_i^0 + \frac{3}{4\pi^2}(1-a_4)\left(\frac{\mu_b}{3}\right)^4 + \sum_{i=u,d,s,e} \mu_i n_i + B_{\text{eff}}, \quad (2)$$

where n_i is the number density for each particle species which can be calculated as

$$n_i = -\left(\frac{\partial \Omega}{\partial \mu_i}\right)_V \quad (3)$$

and the total baryon number density is

$$n_b = \frac{1}{3}(n_u + n_d + n_s). \quad (4)$$

Equilibrium with respect to the weak interactions implies the following relations between the quarks and electron chemical potentials:

$$\mu_s = \mu_d = \mu_u + \mu_e, \quad (5)$$

the electric charge neutrality condition requires:

$$\frac{2}{3}n_u - \frac{1}{3}n_d - \frac{1}{3}n_s - n_e = 0. \quad (6)$$

Since in the present paper we study the case of spinning strange stars, we consider values of the EoS parameters a_4 and B_{eff} so that SQM satisfies the Bodmer–Witten hypothesis. Next, to guarantee the observed stability of atomic nuclei with respect to a possible decay to a droplet of non-strange (i.e. u , d) quark matter, we require that the energy per baryon $(E/A)_{ud}$ of non-strange quark matter should satisfy the condition $(E/A)_{ud} > 930.4 \text{ MeV} + \Delta$, where $\Delta \sim 4 \text{ MeV}$ accounts for finite size effects of the energy per baryon of a droplet of non-strange quark matter with respect to the bulk ($A \rightarrow \infty$) case (Farhi & Jaffe 1984).

The values for the EoS parameters considered in the calculations reported in this work, are listed in Table 1. In particular, to explore the effects of the perturbative QCD corrections on the properties of spinning strange stars, for the fixed value $B_{\text{eff}}^{1/4} = 138 \text{ MeV}$, we consider two different values of the parameter a_4 ($= 0.61$ and 0.80); $a_4 = 0.61$ gives a larger deviation from the ideal gas than $a_4 = 0.80$.

The EoS, for the three parametrizations used in the present work, are plotted in Fig. 1. Notice that at fixed B_{eff} , the value of a_4 has a very small effect on the EoS expressed as $P = P(\varepsilon)$, i.e. pressure P as a function of the energy density ε (left panel in Fig. 1), which enters in the structure equations for non-spinning and spinning stars. To highlight the influence of the perturbative QCD corrections term a_4 on the EoS, in comparison with the EoS 1 and EoS 2, we also plot in Fig. 1 that for the case $B_{\text{eff}}^{1/4} = 138 \text{ MeV}$ and $a_4 = 1.0$ (ideal relativistic Fermi gas plus bag pressure). We do not, however, use this EoS in the calculations for spinning strange stars reported here, since we have verified that for this choice of the parameters $B_{\text{eff}}^{1/4}$ and a_4 , the atomic nuclei are unstable with respect to decay to a droplet of non-strange quark matter.

The results plotted in the left panel of Fig. 1, however, do not imply that the perturbative QCD corrections are unimportant. Clearly, looking at Eq.(1) and the results

plotted in the middle panel of Fig. 1, one sees that the EoS in the form $P(\mu_b) = -\Omega(\mu_b)$ has a sizeable dependence on the parameter a_4 .

The influence of the parameter a_4 on the EoS (Eqs.(1), (2)) of SQM is more clear in the case of massless quarks. In fact, in this case one can show that the EoS for SQM, in a parametrical form in terms of the baryon number density, can be written as:

$$\begin{aligned} \varepsilon &= K n_b^{4/3} + B_{\text{eff}} \\ P &= \frac{1}{3} K n_b^{4/3} - B_{\text{eff}}, \end{aligned} \quad (7)$$

where

$$K = \frac{9}{4} \frac{\pi^{2/3}}{a_4^{1/3}} \quad (8)$$

and eliminating the baryon number density n_b one gets

$$P = \frac{1}{3}(\varepsilon - 4B_{\text{eff}}), \quad (9)$$

which does not depend on a_4 . Thus the stellar gravitational mass M_G versus the central energy density ε_c , or the stellar radius R versus ε_c , in the case of massless quarks, will not depend on the perturbative QCD corrections term a_4 . These stellar properties will have a tiny dependence on a_4 in our case due to the finite value of the strange quark mass, $m_s = 100 \text{ MeV}$. Nevertheless, stellar properties like the total rest mass of the star $M_0(\varepsilon_c)$, the relation between M_G and M_0 and consequently the value of the total stellar binding energy $B = M_0 - M_G$ (Bombaci & Datta 2000) will significantly be affected by the parameter a_4 . This ultimately should affect the energetics of explosive phenomena like supernovae or the conversion of normal neutron stars (nucleonic stars) to strange or hybrid stars (Bombaci & Datta 2000; Berezhiani et al. 2003).

To illustrate how the parameter a_4 affects the stellar rest mass M_0 and binding energy B , let us consider for the moment the case of non-spinning configurations. The stellar rest mass is given by

$$M_0 = m_u \int_0^R 4\pi r^2 n_b(r) \left[1 - \frac{2Gm(r)}{c^2 r}\right]^{-1/2} dr \quad (10)$$

where $m_u = 931.494 \text{ MeV}/c^2$ is the atomic mass unit, $n_b(r)$ is the baryon number density at the radial coordinate r , and $m(r)$ is the stellar gravitational mass enclosed within r . Now, in addition, consider the case of massless quarks. Using Eq.(7) and (8), we get the for the baryon number density

$$n_b(r) = \left(\frac{2}{3}\right)^{3/2} \frac{1}{\sqrt{\pi}} a_4^{1/4} [\varepsilon(r) - B_{\text{eff}}]^{3/4}. \quad (11)$$

Substituting this expression in Eq. (10) and considering that the functions $m(r)$ and $\varepsilon(r)$ do not depend on the parameter a_4 , one obtains the following scaling relation for the stellar rest mass

$$M_0(\varepsilon_c; a_4) = \left(\frac{a_4}{a'_4}\right)^{1/4} M_0(\varepsilon_c; a'_4) \quad (12)$$

where a_4 and a'_4 are two different values of the perturbative QCD corrections parameter and ε_c is the central energy density of the star. Therefore, for a star with a given gravitational mass M_G , the stellar binding energy scales with the

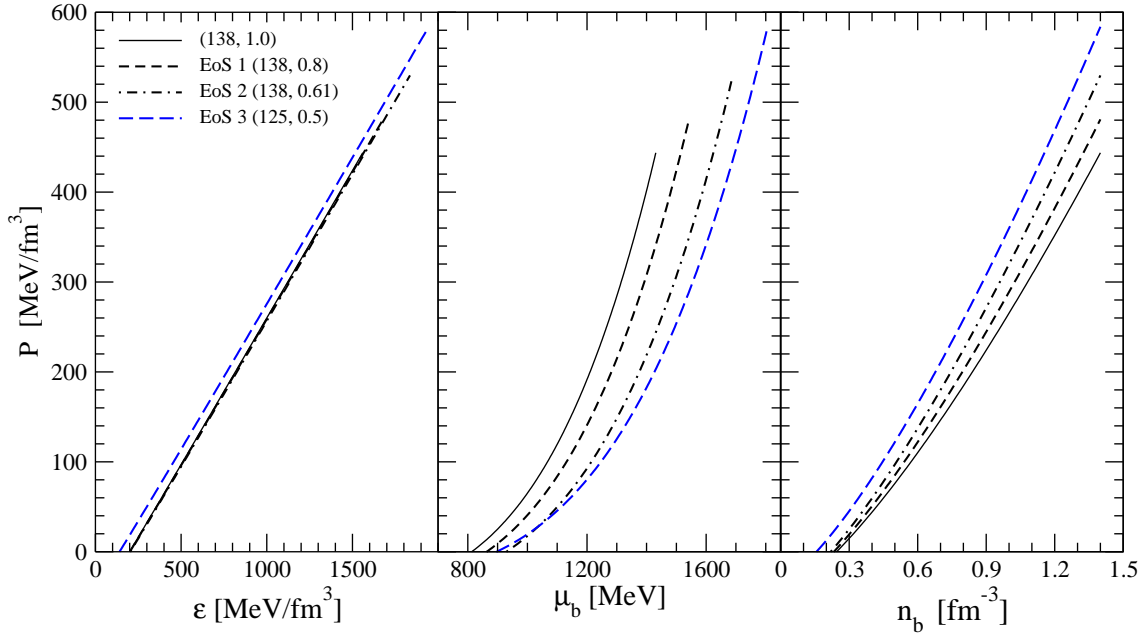


Figure 1. Pressure P versus energy density ε (left panel), P versus baryon chemical potential μ_b (middle panel) and P versus baryon number density n_b (right panel) for the three strange quark matter EoS parameter sets used in the present work (see § 2 and Table 1). To highlight the influence of the perturbative QCD corrections term a_4 on the EoS, in comparison with the EoS 1 and EoS 2 cases, we also plot the EoS with $B_{\text{eff}}^{1/4} = 138$ MeV and $a_4 = 1.0$ (ideal relativistic Fermi gas plus bag pressure).

parameter a_4 as

$$B(a_4) = \left(\frac{a_4}{a'_4}\right)^{1/4} B(a'_4). \quad (13)$$

In Fig. 2 we report our results for the rest mass M_0 of the star as a function of its central density (left panel) and as a function of the corresponding gravitational mass M_G (right panel). Results in Fig. 2 are regarding non-spinning strange stars with the EoS 1 ($a_4 = 0.80$) and EoS 2 ($a_4 = 0.61$) with $B_{\text{eff}}^{1/4} = 138$ MeV in both cases. As we can see, decreasing the value of the parameter a_4 , i.e. increasing the deviation from the ideal relativistic Fermi gas ($a_4 = 1$), results in a reduction of the stellar rest mass at a given central density or at a given M_G . Notice that the results plotted in Fig. 2, for a strange quark mass $m_s = 100$ MeV, are well reproduced by the scaling relation given in Eq. (13). As we will see in the following, this scaling relation will be also very useful in the case of fast spinning stars.

Simple scaling relations for the properties of non-spinning strange stars have been obtained in terms of the effective bag constant B_{eff} (Witten 1984; Haensel et al. 1986; Bombaci 1999; Haensel et al. 2007) in the case of the EoS given by Eq. (9). As discussed in Appendix A, the gravitational mass and the radius of the star, for two different values $B_{\text{eff},1}$ and $B_{\text{eff},2}$ of the effective bag constant, are related by

$$M_G(\varepsilon_{c,1}; B_{\text{eff},1}) = \left(\frac{B_{\text{eff},2}}{B_{\text{eff},1}}\right)^{1/2} M_G(\varepsilon_{c,2}; B_{\text{eff},2}), \quad (14)$$

$$R(\varepsilon_{c,1}; B_{\text{eff},1}) = \left(\frac{B_{\text{eff},2}}{B_{\text{eff},1}}\right)^{1/2} R(\varepsilon_{c,2}; B_{\text{eff},2}), \quad (15)$$

with the two central energy densities satisfying the condition

$$\varepsilon_{c,1}/\varepsilon_{c,2} = B_{\text{eff},1}/B_{\text{eff},2}. \quad (16)$$

Equations (14) and (15) give the scaling law for the mass-radius relation. In particular they hold (Witten 1984; Haensel et al. 1986) for the maximum mass configuration.

Finally, the perturbative QCD corrections to the EoS make it possible to fulfil the Bodmer–Witten hypothesis in a region of the $B_{\text{eff}}^{1/4}$ – a_4 plane where one can get strange stars with a maximum gravitational mass significantly larger than $2 M_\odot$ (see Fig. 1 in Weissenborn et al. (2011)), and thus in agreement with current measurements of compact star masses like that of PSR J1614-2230 ($M = 1.97 \pm 0.04 M_\odot$; Demorest et al. (2010)).

3 COMPUTATION OF RAPIDLY SPINNING STELLAR STRUCTURES

For computing the stationary and equilibrium sequences of strange stars, we make use of the formalism mentioned in Cook et al. (1994); Datta et al. (1998); Bombaci et al. (2000); Bhattacharyya et al. (2000, 2001a,b,c); Bhattacharyya (2002, 2011). The general space-time for such a star is (using $c = G = 1$; Bardeen (1970); Cook et al. (1994)):

$$ds^2 = -e^{\gamma+\rho} dt^2 + e^{2\alpha} (dr^2 + r^2 d\theta^2) + e^{\gamma-\rho} r^2 \sin^2 \theta (d\phi - \omega dt)^2, \quad (17)$$

where γ , ρ , α are metric potentials, ω is the angular speed of the stellar fluid relative to the local inertial frame, and t , r and θ are temporal, quasi-isotropic radial and polar angular coordinates respectively. Assuming the matter comprising

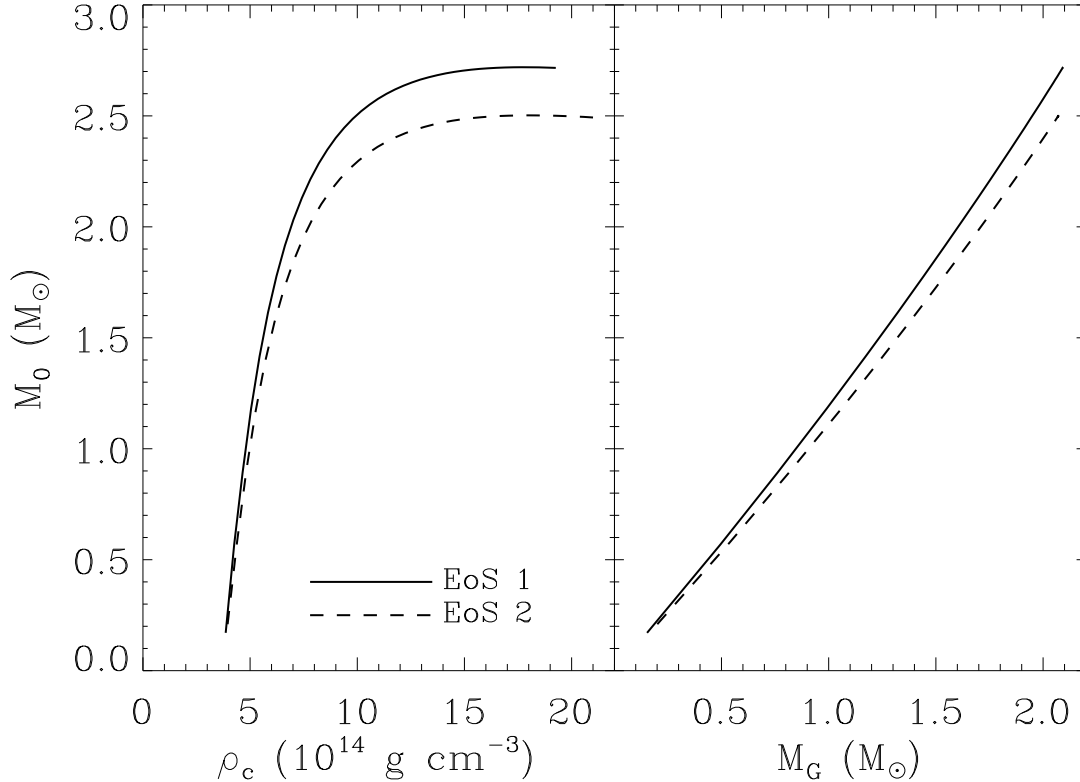


Figure 2. Stellar rest mass M_0 versus central density (left panel), and M_0 versus stellar gravitational mass M_G (right panel) for non-spinning strange stars.

the star to be a perfect fluid with energy momentum tensor:

$$T^{\mu\nu} = (\varepsilon + P)u^\mu u^\nu + P g^{\mu\nu} \quad (18)$$

and a unit time-like description for the four velocity vector we can decompose the Einstein field equations projected onto the frame of reference of a Zero Angular Momentum Observer (ZAMO) to yield three elliptic equations for γ , ρ and ω and a linear ordinary differential equation for α (Cook et al. 1994). The elliptic equations are then converted to integral equations using the Green’s function approach. The hydrostatic equations are derived from the relativistic equations assuming a linear spin law (in our case the spin law integral vanishes for the rigid spin condition). The solution for the hydrostatic equilibrium equation reduces to solving of one algebraic equation at each grid position and matching these with the equatorial values for self-consistency. For a desired central density ρ_c and polar radius to equatorial radius ratio (r_p/r_e), a multi-iteration run of the program to achieve self-consistency yields a 2-dimensional distribution of the metric potentials, density and pressure representing an equilibrium solution. This equilibrium solution is then used to compute compact star parameters, such as gravitational mass (M_G), rest mass (M_0), equatorial circumferential radius (R), total angular momentum (J), spin frequency (ν), moment of inertia (I), total spinning kinetic energy (T), total gravitational energy (W), surface polar redshift (Z_p), and forward (Z_f) and backward (Z_b) redshifts for tangential emission of photons at the equator (Cook et al. 1994; Datta et al. 1998).

Once the equilibrium parameters describing the struc-

ture are obtained, it becomes feasible to compute general quantities exterior to the compact star like the Keplerian angular speed and specifically, the radius r_{ISCO} of the innermost stable circular orbit (ISCO). These quantities depend on the effective potential that has a maximum at r_{ISCO} . Here is how r_{ISCO} is calculated. The radial equation of motion around such a compact star is $\dot{r}^2 \equiv e^{2\alpha+\gamma+\rho}(dr/d\tau)^2 = \tilde{E}^2 - \tilde{V}^2$, where, $d\tau$ is the proper time, \tilde{E} is the specific energy, which is a constant of motion, and \tilde{V} is the effective potential. This effective potential is given by $\tilde{V}^2 = e^{\gamma+\rho}[1 + \frac{l^2/r^2}{e^{\gamma-\rho}}] + 2\omega\tilde{E}l - \omega^2 l^2$, where l is the specific angular momentum and a constant of motion. r_{ISCO} is determined using the condition $\tilde{V}_{,rr} = 0$, where a comma followed by one r represents a first-order partial derivative with respect to r and so on (Thampan & Datta 1998). We consider r_{orb} ($= r_{\text{ISCO}}$) to be the smallest possible radius of the accretion disc. But R is the absolute lower limit of the disc radius. Therefore, if the star extends beyond the ISCO, we set $r_{\text{orb}} = R$ (Bhattacharyya et al. 2000; Bhattacharyya 2011).

Since observations of some pulsars have provided a measure for M_G and ν , we compute constant M_G and constant ν equilibrium sequences of a couple of pulsars. For each EoS model, we also compute a number of constant M_0 sequences. These sequences would represent the evolution of isolated compact stars conserving their rest mass. Such sequences are stable to quasi-radial mode perturbations if $\frac{\partial J}{\partial \rho_c}|_{M_0} < 0$; we calculate the limit where this inequality does not hold.

In addition to this instability limit, there are three other limits: (1) the static or nonspinning limit, where $\nu \rightarrow 0$ and $J \rightarrow 0$; (2) the mass-shed limit, at which the compact star spins too fast to keep matter bound to the surface; and (3) the low-mass limit, below which a compact star cannot form. These four limits together define the stable stellar parameter space for an EoS model (Cook et al. 1994). Here, apart from the instability limit, we calculate the static and mass-shed limit sequences, but we do not attempt to determine the low-mass limit, where the numerical solutions are less accurate (Cook et al. 1994).

4 RESULTS

The results of our computations are summarized in Figs. 3 through 11 and Tables 2 through 7. Figs. 3–5 are for EoS 1, Figs. 6–8 are for EoS 2, and Figs. 9–11 are for EoS 3. Figs. 3, 6 and 9 show M_G versus ρ_c curves. The static limits, which can support maximum M_G values of $2.09 M_\odot$, $2.07 M_\odot$ and $2.48 M_\odot$ for EoS models 1, 2 and 3 respectively, are shown by solid curves. As ρ_c increases, more inward gravitational pull, i.e., more M_G is required to balance the pressure. Apart from the static limit, the mass-shed and instability limit sequences are also shown in these figures (see § 3). The star is not stable for the parameter space to the right of the curve defining the instability limit. A number of constant rest mass sequences, and the $M_G = 1.97 M_\odot$ sequence are also shown in Figs. 3, 6 and 9. On a constant rest mass sequence, the stellar J increases from right to left, and so does M_G to balance the extra centrifugal force. The rest mass sequence, which joins the maximum M_G on the static limit, separates the supramassive sequence region (above) from the normal sequence region (below). In the supramassive region, a compact star is so massive that it can be stable only if it has sufficient J value. When J decreases (say, via electromagnetic and/or gravitational radiation) to the value corresponding to the instability limit, the compact star collapses further to become a black hole. Another surprising aspect of the supramassive region is, as J decreases, I can decrease at a higher rate, and hence ν can increase. So the star can spin up, as it loses angular momentum.

Figs. 4, 7 and 10 show M_G versus R curves for various sequences. These figures show that R usually increases with M_G . This property distinguishes strange stars from “normal” neutron stars (see also § 1). Figs. 5, 8 and 11 show ν versus dimensionless J (cJ/GM_\odot^2) curves. These figures clearly show, while ν decreases with the decrease of J in the normal sequence region, it can have opposite behaviour in the supramassive region. Finally, we note that all the curves of the Figs. 3–11 are qualitatively consistent with those for other SQM EoS models (see, for example, Bombaci et al. (2000)).

Table 2 displays the values of ρ_c , M_0 , R , R/r_g and r_{orb} for the maximum M_G configurations in static limit. This table shows that the stellar radius is $3.74r_g$ ($3.75r_g$, $3.75r_g$) and the ISCO is ~ 7 (~ 7 , ~ 8) km above the compact star for EoS 1 (2, 3). Here, r_g is the Schwarzschild radius. For the mass-shed limit, the maximum values of M_G , J and ν are $3.03 M_\odot$, $7.17 \times 10^{49} \text{ g cm}^2 \text{ s}^{-1}$ and $\sim 1500 \text{ Hz}$ respectively for EoS 1, $3.00 M_\odot$, $7.01 \times 10^{49} \text{ g cm}^2 \text{ s}^{-1}$ and $\sim 1501 \text{ Hz}$ respectively for EoS 2, and are $3.60 M_\odot$, $9.98 \times 10^{49} \text{ g cm}^2$

s^{-1} and $\sim 1250 \text{ Hz}$ respectively for EoS 3 (see Tables 3 and 4). But note that these three numbers for a given EoS model are for three different configurations on the mass-shed limit sequence. Tables 3 and 4, which display the stable parameter values for maximum values of M_G and J respectively, show that there is a gap of almost 2 km between the star and the ISCO, and T/W is roughly 0.21 for each EoS model.

Table 5 displays three configurations on the rest mass $M_0 = 2.00 M_\odot$ sequence for EoS 1 and EoS 2. These configurations are also marked with filled circles in Figs. 3–8. This table shows that, for the same ρ_c , most of the parameters have significantly different values for the two EoS models. This difference is around or more than one order of magnitude for J , ν and T/W for the highest ρ_c value considered.

After this general characterisation of the SQM EoS models for rapidly spinning stars, we compute the stable structures of two well known pulsars. We show the parameter values for the massive pulsar PSR J1614-2230 ($M_G = 1.97 M_\odot$, $\nu = 317.5 \text{ Hz}$; § 1) for the three EoS models in Table 6. This pulsar is marked with a square symbol in each of Figs. 3–11. The mass of the fastest known pulsar PSR J1748-2446ad ($\nu = 716 \text{ Hz}$; § 1) is not yet known. We, therefore, compute the $\nu = 716 \text{ Hz}$ equilibrium sequences for the three EoS models, and show the stable stellar parameter values for a number of configurations in Table 7. The maximum values of M_G supported by $\nu = 716 \text{ Hz}$ are $2.18 M_\odot$, $2.16 M_\odot$ and $2.64 M_\odot$ for EoS models 1, 2 and 3 respectively. Figs. 3–11 show the $\nu = 716 \text{ Hz}$ sequence with long-dashed curves and the maximum M_G configuration with a diamond symbol on each of these curves.

5 DISCUSSION

In this paper, we confirm that strange stars with interacting quark matter can support $> 2M_\odot$ gravitational mass, even when they are not spinning. Since the highest precisely measured masses of compact stars are $\approx 2M_\odot$ (see § 1; also Antoniadis et al. (2013)), this provides a possibility of the existence of strange stars. In order to explore this possibility, here we consider three EoS models based on MIT bag model with perturbative corrections due to quark interactions (§ 2). These EoS models are characterized by an effective bag constant (B_{eff}) and a perturbative QCD corrections term (a_4). We, for the first time, compute rapidly spinning strange star equilibrium sequences for these models, which are essential to study millisecond pulsars, as well as non-pulsar fast spinning compact stars in LMXB systems (§ 1). We find that the maximum masses supported by our EoS models are in the range $3.0 - 3.6 M_\odot$ for the mass-shed limit, and in the range $\approx 2.2 - 2.6 M_\odot$ for the spin frequency ($\nu = 716 \text{ Hz}$) of the fastest known pulsar. Hence, a precise measurement of a high mass will be required to reject these EoS models based on mass measurement alone. The maximum spin frequency of $\approx 1250 - 1500 \text{ Hz}$ can be supported by EoS 1 – 3 (§ 4). Therefore, spin-down mechanisms, such as those due to disk-magnetosphere interaction (Burderi et al. 1999; Ghosh 1995), electromagnetic radiation (Ghosh 1995) and/or gravitational radiation (Bildsten 1998), may be required to explain the absence of an observed spin frequency above 716 Hz. The spin-down due to disk-magnetosphere interaction can happen for both accret-

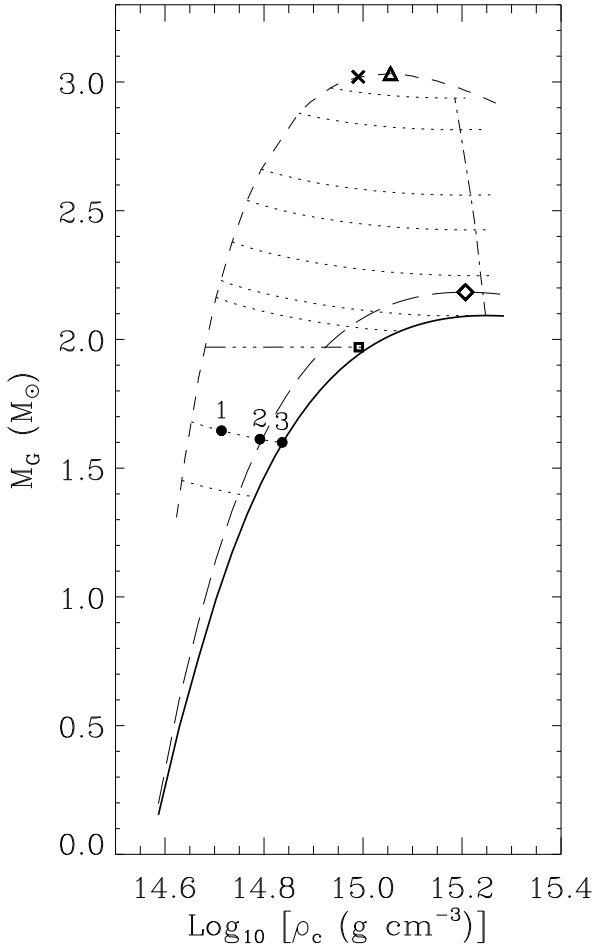


Figure 3. Gravitational mass versus central density plot of strange stars for EoS 1 (see § 2 and Fig. 1). The solid curve is for a non-spinning star, the short-dashed curve shows the mass-shed limit, the long-dashed curve is for a spin frequency of 716 Hz, the dotted curves are for evolutionary (i.e., constant rest mass) sequences, the dash-dot curve gives the instability limit to quasi-radial mode perturbations, and the dash-triple-dot curve is for the gravitational mass = 1.97 M_{\odot} . The constant rest mass values, for dotted curves from bottom to top, are 1.71 M_{\odot} , 2.00 M_{\odot} , 2.63 M_{\odot} , 2.72 M_{\odot} , 2.92 M_{\odot} , 3.15 M_{\odot} , 3.33 M_{\odot} , 3.66 M_{\odot} and 3.82 M_{\odot} . The triangle and cross symbols are for the maximum mass (Table 3) and the maximum total angular momentum (Table 4) respectively for the mass-shed sequence, the three filled circles marked with ‘1’, ‘2’ and ‘3’ on the rest mass sequence $M_0 = 2.00 M_{\odot}$ correspond to the ‘No.’ column of Table 5, the square symbol is for the observed mass (= 1.97 M_{\odot}) and spin frequency (= 317.5 Hz) of PSR J1614-2230 (Table 6), and the diamond symbol is for the maximum mass which can be supported by the fastest known pulsar PSR J1748-2446ad spinning at 716 Hz (Table 7). See § 4 for a description.

ing “normal” neutron stars and strange stars, if the spin-down in the propeller regime is more than the spin-up in the accretion regime (Burderi et al. 1999). The electromagnetic radiation and the gravitational radiation exert negative torques $\propto \nu^3$ and $\propto \nu^5$ respectively on the compact star (Ghosh 1995; Bildsten 1998). These two latter mecha-

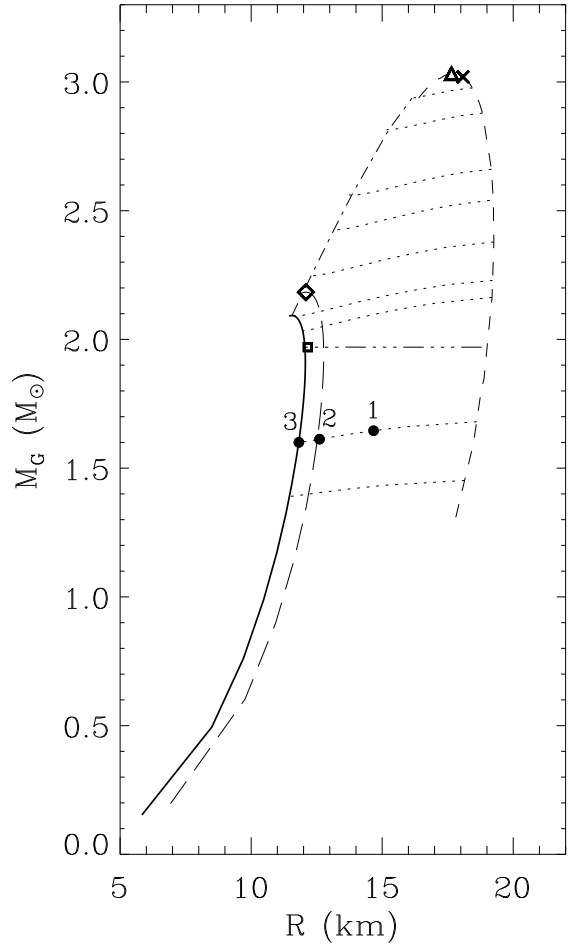


Figure 4. Gravitational mass versus equatorial radius plot of strange stars for EoS 1 (see § 2 and Fig. 1). The meanings of curves and symbols are same as in Fig. 3.

nisms can also work for strange stars (Ahmedov et al. 2012; Andersson et al. 2002).

We note that the maximum angular momentum appears at a lower central density than that for the maximum mass (Tables 3 and 4). This is in agreement with calculations for other EoS models (Bombaci et al. 2000). A comparison between EoS 1–2 and EoS 3 for the maximum mass or maximum angular momentum configurations gives some idea about the extent of the dependence of stellar parameter values on the EoS model parameter B_{eff} (Tables 2–4). Here we list some of the points. (1) The central density is significantly lower for the lower effective bag constant (B_{eff}) value (i.e., EoS 3). This general behaviour is in agreement with the scaling law Eq. (16) mentioned in § 2 (see also § A). (2) A lower effective bag constant value can support a larger mass, and the corresponding radius is also higher. These are expected from the scaling law Eqs. (14) and (15), especially for maximum mass configurations of non-spinning compact stars with EoS model given in Eq. (9) (§ 2; see also § A). We find that, for our EoS 2 and EoS 3, the mass ratio and the radius ratio expected from Eqs. (14) and (15) hold within a few percent not only for non-spinning maximum

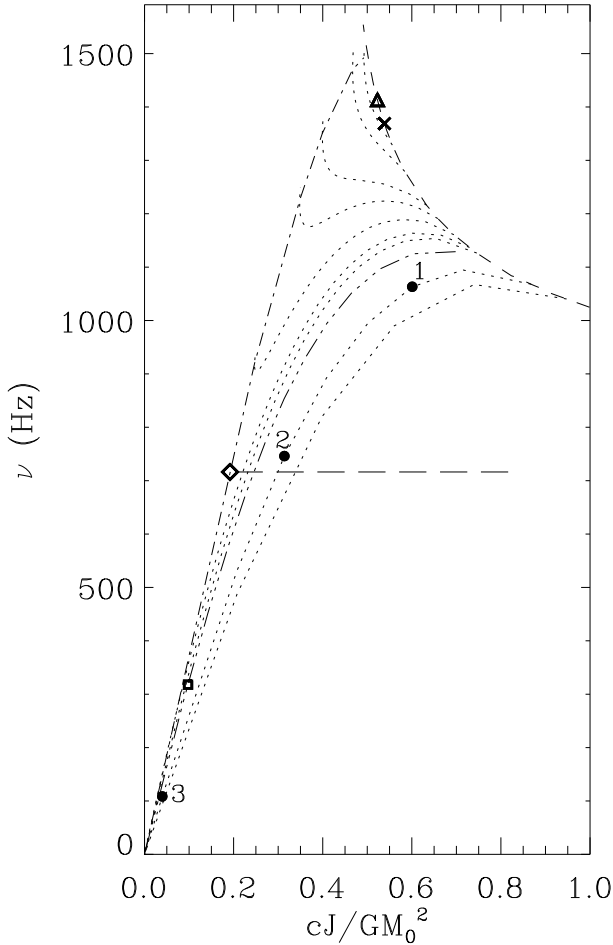


Figure 5. Spin frequency versus dimensionless angular momentum plot of strange stars for EoS 1 (see § 2 and Fig. 1). J is the total angular momentum and M_0 is the rest mass. The meanings of curves and symbols are same as in Fig. 3.

mass configurations (Table 2), but also for mass-shed limit maximum mass configurations (Table 3). As a result, the stellar compactness, which is the mass-to-radius ratio, and hence the surface redshift values, are somewhat similar for all B_{eff} values. (3) T/W weakly depends on B_{eff} , and the value is ~ 0.21 for maximum mass and maximum angular momentum configurations. At this value, the compact star could be susceptible to triaxial instabilities (Bombaci et al. 2000). (4) The oblateness of the compact star, as inferred from R_p/R ($\sim 0.53 - 0.55$), is a weak function of B_{eff} . (5) J and I strongly decreases, while ν significantly increases, with the increase of B_{eff} . The strong B_{eff} -dependence of I is expected from the scaling law equations 14 and 15 (§ 2; see also § A), because $I \sim M_G R^2$. We verify that ν roughly scales with $B_{\text{eff}}^{1/2}$ (Table 3), as expected (see § A). Since $J \propto I\nu$, J is expected to scale with B_{eff}^{-1} , which we verify (Table 3). (6) The two different situations, viz., $r_{\text{ISCO}} > R$ and $r_{\text{ISCO}} < R$ (r_{ISCO} is ISCO radius) have important consequences for observed X-ray features, and hence on the measurements of compact star parameters (e.g., Bhattacharyya (2011)). In the former situation, the length of the gap between r_{ISCO}

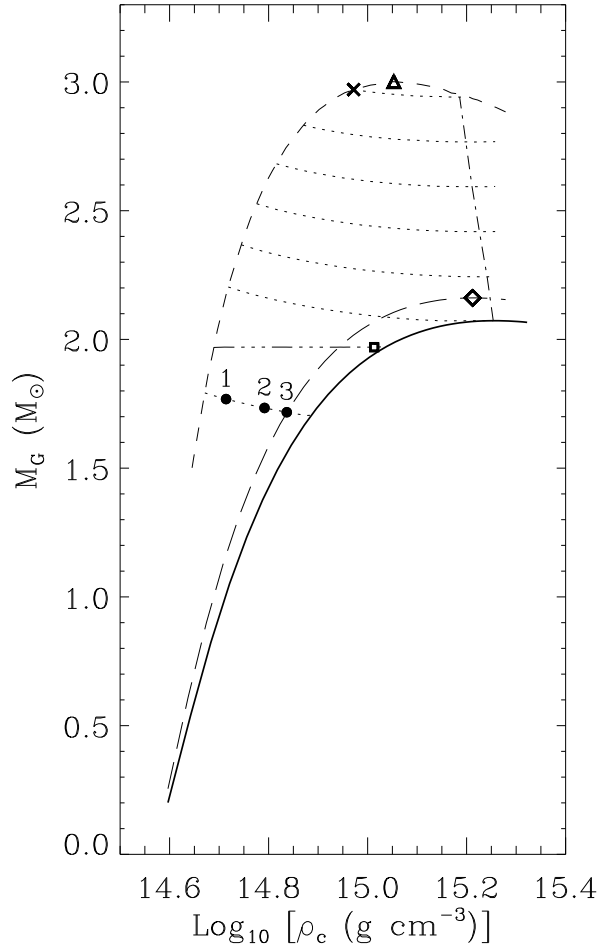


Figure 6. Gravitational mass versus central density plot of strange stars for EoS 2 (see § 2 and Fig. 1). The meanings of curves and symbols are same as in Fig. 3. The constant rest mass values, for dotted curves from bottom to top, are $2.00 M_\odot$, $2.50 M_\odot$, $2.71 M_\odot$, $2.92 M_\odot$, $3.13 M_\odot$, $3.34 M_\odot$, and $3.55 M_\odot$.

and R is also very important for the X-ray emission, because the boundary layer emission to the accretion disc emission ratio depends on this length (e.g., Bhattacharyya et al. (2000)). We find that r_{ISCO} is greater than R for the maximum mass and maximum angular momentum configurations, and the gap-length for EoS 1–2 is somewhat lower than that for EoS 3. This is expected from the scaling law equations 14 and 15 (§ 2; see also § A), because $r_{\text{ISCO}} \propto M_G$.

Let us now examine how B_{eff} can be constrained from observations, especially when M_G and ν have been measured. Comparing EoS 2 ($B_{\text{eff}}^{1/4} = 138$ MeV) and EoS 3 ($B_{\text{eff}}^{1/4} = 125$ MeV), we find significant differences for the measurable parameters R/r_g , R and I , which are $\approx 17\%$, $\approx 17\%$ and $\approx 31\%$ respectively (Table 6). Note that, since these parameters depend on a_4 only very weakly (see row 1 and row 2 of Table 6), the relatively small a_4 difference between EoS 2 and EoS 3 does not prohibit us to study a B_{eff} dependence.

In order to examine if the above quoted differences are in agreement with the scaling laws mentioned in § A, even

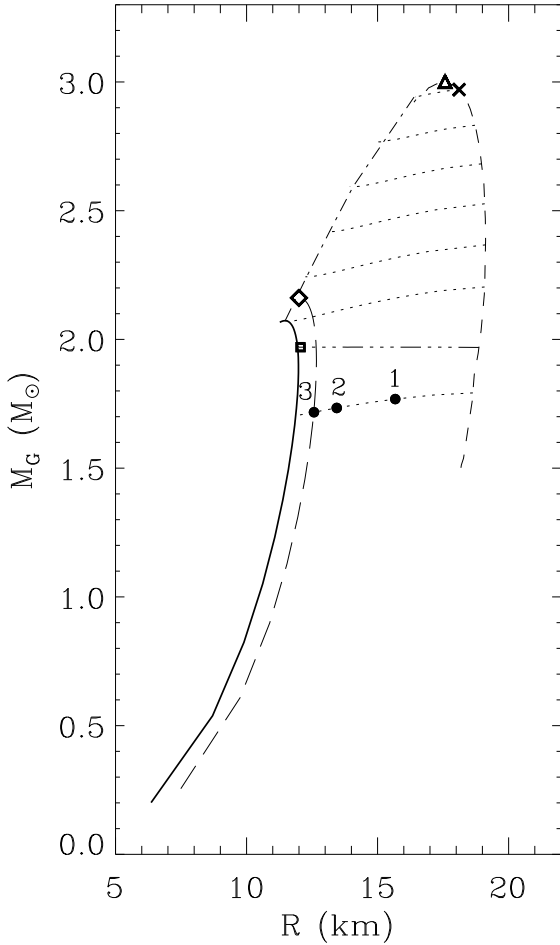


Figure 7. Gravitational mass versus equatorial radius plot of strange stars for EoS 2 (see § 2 and Fig. 1). The meanings of curves and symbols are same as in Fig. 3.

for a fast spinning star for which the TOV equations (A4 and A5) are not exactly valid, first we mention the ratios of R/r_g , R and I for $B_{\text{eff}}^{1/4} = 138$ MeV and $B_{\text{eff}}^{1/4} = 125$ MeV. These are $[R/r_g]_{\text{EoS2}}/[R/r_g]_{\text{EoS3}} = 0.84$, $R_{\text{EoS2}}/R_{\text{EoS3}} = 0.84$, and $I_{\text{EoS2}}/I_{\text{EoS3}} = 0.73$ (Table 6). Now, since radius is a weak function of central density for most of the observationally relevant portion of the parameter space (say, $M_G > 1M_\odot$; see, for example, Figs. 3 and 4), we can assume $R \propto B_{\text{eff}}^{-1/2}$ from Eq. A7, and hence we expect $R_{\text{EoS2}}/R_{\text{EoS3}} \approx 0.82$, which is close to the above mentioned value. Note that M_G is constant for all EoS models in Table 6. Therefore, while comparing parameter values for EoS 2 and EoS 3, we expect $R/r_g \propto R \propto B_{\text{eff}}^{-1/2}$ and $I \propto R^2 \propto B_{\text{eff}}^{-1}$. Hence from § A we expect $[R/r_g]_{\text{EoS2}}/[R/r_g]_{\text{EoS3}} = 0.82$ and $I_{\text{EoS2}}/I_{\text{EoS3}} = 0.67$, which are close to the above mentioned values.

So let us now see if some of the above quoted percentage differences of R/r_g , R and I (Table 6) can be observationally measured. A fortuitous discovery of an atomic spectral line can constrain R/r_g with better than 5% accuracy, even when the star is rapidly spinning making the line broad and skewed (Bhattacharyya et al. 2006). Other meth-

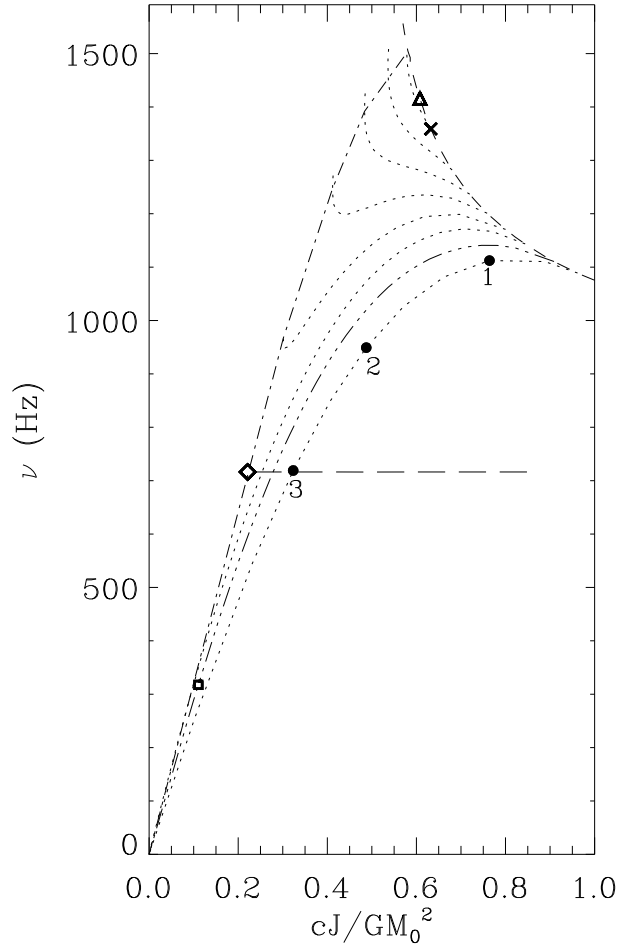


Figure 8. Spin frequency versus dimensionless angular momentum plot of strange stars for EoS 2 (see § 2 and Fig. 1). J is the total angular momentum and M_0 is the rest mass. The meanings of curves and symbols are same as in Fig. 3.

ods to measure R/r_g are also available (e.g., Bhattacharyya (2010), Bhattacharyya et al. (2005)). Possible measurements of R for LMXBs and the related difficulties have been discussed in a number of papers (e.g., Güver et al. (2012a,b); Steiner et al. (2010, 2013); Suleimanov et al. (2011a,b); Guillot & Rutledge (2014)). Modelling of burst oscillations observed with a future large area X-ray timing instrument can tightly constrain R of a compact star in an LMXB (Lo et al. 2013). The pulsed X-ray emission from radio millisecond pulsars can also be useful to constrain R (Bogdanov & Grindlay 2009; Bogdanov et al. 2008; Özel et al. 2015). In fact, the upcoming *NICER* space mission is expected to measure the R of the nearest and best-studied millisecond pulsar PSR J0437-4715 with 5% accuracy. Besides, a measurement of I of the binary pulsar J0737-3039A with 10% accuracy has been talked about (Morrison et al. 2004). Apart from R/r_g , R and I , $[r_{\text{orb}} - R]$ of LMXBs, which can be inferred from spectral and timing studies of observed X-ray emission (e.g., Bhattacharyya et al. (2000)), also has a significant difference ($\approx 98\%$) between EoS 2 and EoS 3. Therefore, since

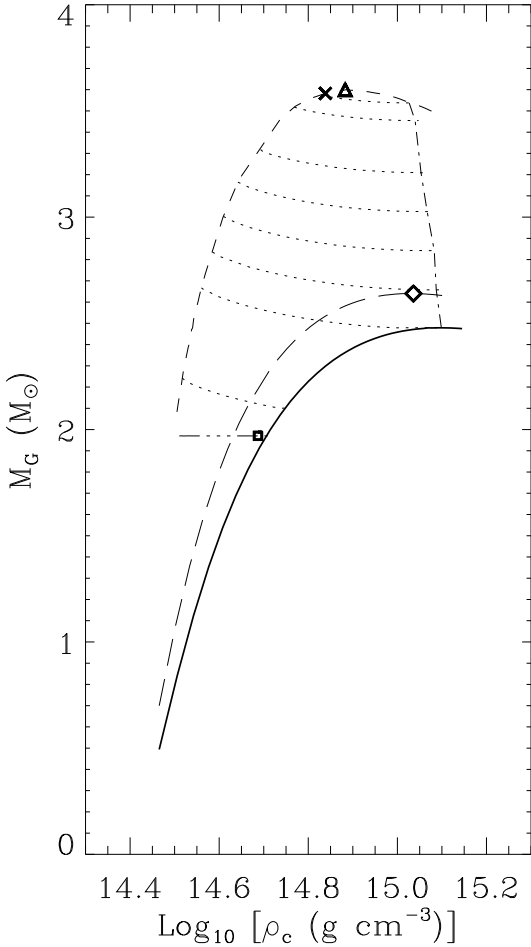


Figure 9. Gravitational mass versus central density plot of strange stars for EoS 3 (see § 2 and Fig. 1). The meanings of curves and symbols are same as in Fig. 3. The constant rest mass values, for dotted curves from bottom to top, are $2.54 M_{\odot}$, $3.09 M_{\odot}$, $3.32 M_{\odot}$, $3.54 M_{\odot}$, $3.77 M_{\odot}$, $4.00 M_{\odot}$, $4.30 M_{\odot}$, and $4.40 M_{\odot}$.

M_G and ν have been measured for a number of compact stars (see § 1), B_{eff} could be constrained from observations, within the ambit of our EoS models.

After discussing how B_{eff} could be constrained, let us now study the possible effects of the perturbative QCD corrections term a_4 on stellar parameters. In order to do this, we compare the stellar properties for EoS 1 & EoS 2 for a constant rest mass sequence $M_0 = 2.00 M_{\odot}$ (Table 5). This is the sequence along which a non-accreting compact star evolves. We consider such a sequence for comparison, because the a_4 value is expected to affect M_0 and the total stellar binding energy B (see § 2). We verify this for three central density values (Table 5). For all these densities, B for $a_4 = 0.80$ is $\approx 0.12 M_{\odot}$ higher than B for $a_4 = 0.61$.

As a result, a_4 could have signatures in evolution of compact star and other system properties, within the ambit of our EoS models. For example, the evolution of non-accreting compact stars happens keeping the M_0 value constant, while the other parameters evolve depending on the

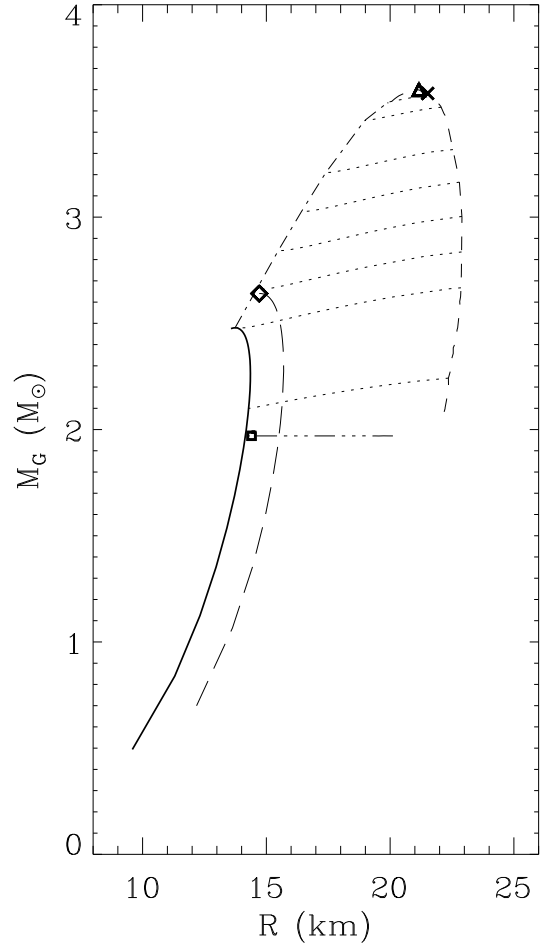


Figure 10. Gravitational mass versus equatorial radius plot of strange stars for EoS 3 (see § 2 and Fig. 1). The meanings of curves and symbols are same as in Fig. 3.

a_4 parameter (Table 5). For accreting compact stars, the increase of M_G for a certain amount of added M_0 depends on B , and hence on a_4 . Besides, orbital period (P_{orb}) evolution of LMXBs depends on, among other things, the fraction of exchanged matter lost from the binary system (see equation 3.14 of Bhattacharya & van den Heuvel (1991)). Therefore, as an amount of matter ΔM_0 from the companion star falls on the compact star, the system loses a mass $\Delta M_0 - \Delta M_G$. This is because the transferred matter becomes bound to the compact star, and $\Delta M_G < \Delta M_0$. This difference (i.e., the corresponding binding energy) is released from the system. The amount of this lost mass, which affects P_{orb} , increases with B , and hence with a_4 . Furthermore, Sudden mass loss can happen when the core of a massive star collapses into a compact star, or when a “normal” neutron star (nucleonic star) changes into a strange or a hybrid star (Berezhiani et al. 2003), and the star loses gravitational mass as it becomes more bound. Therefore, B of the final stellar configuration, which will depend on a_4 if the final star contains interacting quark matter, will influence the stellar parameter values (e.g., M_G , ν) after collapse. If such a collapsed star is in a binary system, then B (and

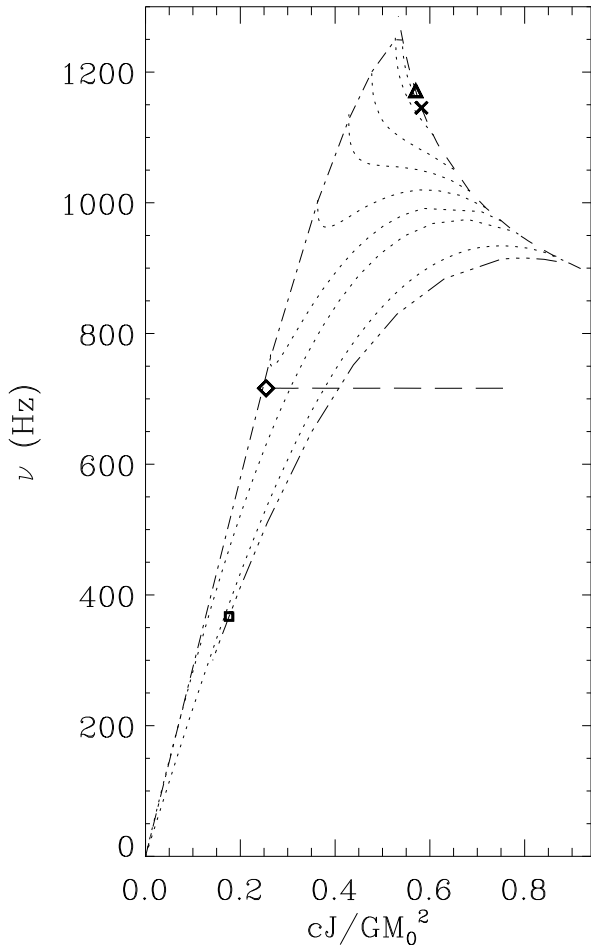


Figure 11. Spin frequency versus dimensionless angular momentum plot of strange stars for EoS 3 (see § 2 and Fig. 1). J is the total angular momentum and M_0 is the rest mass. The meanings of curves and symbols are same as in Fig. 3.

hence a_4) may also significantly affect P_{orb} and the orbital eccentricity (Flannery & van den Heuvel 1975).

Therefore, a_4 can be an important ingredient for the computations of stellar evolution and binary evolution. Hence the comparison of the results of such computations with the measured distribution of M_G , ν , P_{orb} and other source parameter values holds the potential to constrain a_4 . However, a reliable constraint may be possible, if the systematic uncertainties due to various unknown source parameters and less understood processes (e.g., disc-magnetosphere interaction) are sufficiently reduced.

Table 6 is additionally useful, because it lists a number of parameter values of an important pulsar for our EoS models. These values will not only be useful to constrain EoS models, but also be important to model the accretion and binary evolution process that created this pulsar. Given the high stellar mass of this source, such a modelling will be useful to address important problems such as the possibility of high birth mass of compact stars.

Table 7 lists a number of parameter values of another pulsar PSR J1748-2446ad. This is the fastest known pul-

sar, and hence is of immense importance (§ 1). However, the mass of PSR J1748-2446ad is not known, and hence we compute several stable stellar configurations for each EoS model, keeping ν at the observed value. These numbers characterize the compact star, and will be useful to study the evolution that created this pulsar. This study can be important to address problems such as why we do not observe a compact star spin frequency higher than a certain value.

6 SUMMARY

Here we summarize the key points of this paper.

(1) We explore the possibility of the existence of strange stars using three EoS models based on MIT bag model with perturbative corrections due to quark interactions. We, for the first time, compute the equilibrium sequences of fast spinning strange stars for these EoS models.

(2) Our EoS models can support maximum gravitational mass values in the range $\approx 3.0 - 3.6M_\odot$, and maximum spin frequencies in the range $\approx 1250 - 1500$ Hz. Thus these EoS models are consistent with the maximum measured mass ($\approx 2.0M_\odot$) and the highest observed spin frequency (716 Hz) of compact stars.

(3) Our EoS models are characterized by two parameters: (a) an effective bag constant (B_{eff}), and (b) a perturbative QCD corrections term (a_4). We study the effects of these two parameters on measurable compact star properties. This could be useful to find possible ways to constrain these fundamental quark matter parameters from observations within the ambit of interacting quark matter EoS models.

(4) Effects of B_{eff} : we find that a higher stellar mass is allowed for a lower B_{eff} value. Furthermore, for a compact star with known gravitational mass and spin frequency, other measurable parameters, such as stellar radius, radius-to-mass ratio and moment of inertia, sufficiently increase with the decrease of B_{eff} . These are primarily a consequence of the scaling laws quoted in § A as discussed in § 5. Such effects of B_{eff} can be useful to constrain the effective bag constant, as mass and spin of compact stars are measurable.

(5) Effects of a_4 : we find that a_4 significantly affects the stellar rest mass and the total stellar binding energy. Therefore, a_4 could have signatures in evolutions of both accreting and non-accreting compact stars, orbital period evolution of LMXBs, sudden mass loss via collapse, and hence the observed distribution of stellar mass and spin, orbital period and other source parameters.

(6) We compute observationally measurable and other parameter values of two important pulsars: PSR J1614-2230 and PSR J1748-2446ad for our EoS models. The first one has the highest precisely measured mass with < 10 ms spin period, and the second one has the highest measured spin frequency. Our reported numbers should be useful ingredients for computations of their evolutionary histories, as well as for constraining EoS models from their future observations.

ACKNOWLEDGEMENTS

We thank an anonymous referee for the constructive comments, which improved the paper.

REFERENCES

- Ahmedov B.J., Ahmedov B.B., Abdurjabbarov A.A., 2012, *Astrophys Space Sci*, 338, 157
- Alcock C., Farhi E., Olinto A., 1986, *ApJ*, 310, 261
- Alford M., Braby M., Paris M., Reddy S., 2005, *ApJ*, 629, 969
- Andersson N., Jones D. I., Kokkotas K.D., 2002, *MNRAS*, 337, 1224
- Andersson N., Ferrari V., Jones D. I., Kokkotas K.D., Krishman B., Read J.S., Rezzolla L., Zink B., 2011, *Gen. Relat. Grav.*, 43, 409
- Antoniadis J. et al., 2013, *Science*, 340, 448
- Aoki Y., Endrodi G., Fodor Z., Katz S. D., Szabó K. K., 2006, *Nature*, 443, 675
- Baade W, Zwicky F., 1934, *Phys. Rev.*, 45, 138
- Baluni V., 1978, *Phys. Rev. D*, 17, 2092
- Bardeen J. M., 1970, *ApJ*, 162, 71
- Bazavov A. et al., 2012, *Phys. Rev. D*, 85, 054503
- Benhar O., Ferrari V., Gualtieri L., Marassi S., 2007, *Gen. Relat. Grav.*, 39, 1323
- Berezhiani Z., Bombaci I., Drago A., Frontera F., Lavagno A., 2002, *Nucl. Phys. B - Proc. Suppl*, 113, 268
- Berezhiani Z., Bombaci I., Drago A., Frontera F., Lavagno A., 2003, *ApJ*, 586, 1250
- Bernard C. et al., 2005, *Phys. Rev. D*, 71, 034504
- Bhattacharya D., van den Heuvel E. P. J., 1991, *Physics Reports*, 203, 1
- Bhattacharyya S., 2002, *A&A*, 383, 524
- Bhattacharyya S., 2010, *Advances in Space Research*, 45, 949
- Bhattacharyya S., 2011, *MNRAS*, 415, 3247
- Bhattacharyya S., Thampan A. V., Misra R., Datta B., 2000, *ApJ*, 542, 473
- Bhattacharyya S., Bhattacharya D., Thampan A. V., 2001, *MNRAS*, 325, 989
- Bhattacharyya S., Misra R., Thampan A. V., 2001, *ApJ*, 550, 841
- Bhattacharyya S., Thampan A. V., Bombaci I., 2001, *A&A*, 372, 925
- Bhattacharyya S., Strohmayer T. E., Miller M. C., Markwardt, C. B., 2005, *ApJ*, 619, 483
- Bhattacharyya S., Miller M. C., Lamb F. K., 2006, *ApJ*, 644, 1085
- Bildsten L., 1998, *ApJ*, 501, L89
- Bodmer A. R., 1971, *Phys. Rev. D*, 4, 1601
- Bogdanov S., Grindlay J. E., 2009, *ApJ*, 703, 1557
- Bogdanov S., Grindlay J. E., Rybicki G.B., 2009, *ApJ*, 689, 407
- Bombaci I., 1999, *Nuclear Methods and the Nuclear Equation of State*, *International Review of Nuclear Physics* 8, World Scientific, p.381
- Bombaci I., 2007, *Eur. Phys. J. A* 31, 810
- Bombaci I., Datta B., 2000, *ApJ*, 530, L69
- Bombaci I., Logoteta D., 2013, *MNRAS*, 433, L79
- Bombaci I., Parenti I., Vidaña I., 2004, *ApJ*, 614, 314
- Bombaci I., Prakash M., Prakash M., Ellis P. J., Lattimer J. M., Brown G. E., 1995, *Nucl. Phys. A*, 583, C623
- Bombaci I., Thampan A. V., Datta B., 2000, *ApJ*, 541, L71
- Bombaci I., Lugones G., Vidaña I., 2007, *A&A*, 462, 1017
- Bombaci I., Logoteta D., Providência C., Vidaña I., 2011, *A&A*, 528, A71
- Borsanyi S. et al, 2010, *J. High Energy Phys.*, 09, 073
- Burderi L., Possenti A., Colpi M., Di Salvo, T., D'Amico N., 1999, *ApJ*, 519, 285
- Burrows A., Lattimer J. M. 1986, *ApJ*, 307, 178
- Cheng M. et al., 2006, *Phys. Rev. D*, 74, 054507
- Chodos A., Jaffe R. L., Johnson K., Thorn C. B., Weisskopf V. F., 1974, *Phys. Rev. D*, 9, 3471
- Cook G. B., Shapiro S. L., Teukolsky S. A., 1994, *ApJ*, 424, 823
- Datta B., Thampan A. V., Bombaci I., 1998, *A&A*, 334, 943
- Demorest P., Pennucci T., Ransom S., Roberts M., Hessels J., 2010, *Nature*, 467, 1081
- Di Giacomo A., Dosch H. G., Shevchenko V. I., Simonov Y. A., 2002, *Phys. Rep.*, 372, 319
- Dosch H. G., 1987, *Phys. Lett. B*, 190, 177
- Dosch H. G., Simonov Yu., 1988, *Phys. Lett. B* 205, 339
- Farhi E., Jaffe R. L., 1984, *Phys. Rev. D*, 30, 272
- Flannery B. P., van den Heuvel E. P. J., 1975, *A&A*, 39, 61
- Fraga E., Pisarki R.D., Schaffner-Bielich J., 2001, *Phys. Rev. D*, 63, 121702(R)
- Fraga E., Kurkela A., Vuorinen A., 2014, *ApJ*, 781, L25
- Freedman B. A., McLerran L. D., 1977, *Phys. Rev. D*, 16, 1130
- Freedman B. A., McLerran L. D., 1978, *Phys. Rev. D*, 17, 1109
- Fu W.-J., Wei H.-Q., Liu Y.-X., 2008, *Phys. Rev. Lett.*, 101, 181102
- Ghosh P., 1995, *Journal of Astrophysics and Astronomy*, 16, 289
- Guillot S., Rutledge R. E., 2014, *ApJ*, 796, L3
- Güver T., Psaltis D., Özel F., 2012, *ApJ*, 747, 76
- Güver T., Özel F., Psaltis D., 2012, *ApJ*, 747, 77
- Haensel P., Zdunik J. L., Schaefer R., 1986, *A&A*, 160, 121
- Haensel P., Potekhin A. Y., Yakovlev D. G., 2007, *Neutron Stars*, Springer
- Han K., Ashenfelter J., Chikarian A., Emmet W., Finch L. E., Heinz A., Madsen J., Majka R. D., Monreal B., Sandweiss J., 2009, *Phys. Rev. Lett.*, 103, 092302
- Hessels J. W. T., Ransom S. M., Stairs I. H., Freire P. C. C., Kaspi V. M., Camilo F., 2006, *Science*, 311, 1901
- Hewish A., Bell S. J., Pilkington J. D. H., Scott P. F., Collins R. A., 1968, *Nature*, 217, 709
- Kurkela A., Romatschke P., Vuorinen A., 2010, *Phys. Rev. D*, 81, 105021
- Lattimer J. M., Prakash M., 2001, *ApJ* 550, 246
- Li X.-D., Bombaci I., Dey M., Dey J., van den Heuvel E. P. J., 1999, *Phys. Rev. Lett.*, 83, 3776
- Li X.-D., Ray S., Dey J., Dey M., Bombaci I., 1999, *ApJ*, 527, L51
- Lo K. H., Miller M. C., Bhattacharyya S., Lamb F. K., 2013, *ApJ*, 776, 19
- Logoteta D., Bombaci I., 2013, *Phys. Rev. D*, 88, 061001
- Morrison I. A., Baumgarte, T. W., Shapiro, S. L., Pandharipande, V. R., 2004, *ApJ*, 617, L135
- Nefediev A. V., Simonov Yu. A., Trusov A. M., 2009, *Int. Jour. Mod. Phys. E*, 18, 549
- Nishimura N. et al., 2012, *ApJ*, 758, 9
- Özel F., Psaltis D., Arzoumanian Z., Morsink S., Baubock M., 2015, submitted (arXiv:1512.03067)
- Patruno A., Watts A. L., 2012, in *Timing neutron stars: pulsations, oscillations and explosions*, eds. T. Belloni, M. Mendez, C. M. Zhang, ASSL, Springer
- Perez-Garcia M. A., Silk J., Stone J. R., 2010, *Phys. Rev. Lett.*, 105, 141101
- Prakash M., Bombaci I., Prakash M., Ellis P. J., Lattimer J. M., Knorren R., 1997, *Phys. Rep.* 280, 1
- Rupak G., Prashanth Jaikumar P., 2013, *Phys. Rev. C* 88, 065801
- Simonov Yu., 1988, *Nucl. Phys. B*, 307, 512
- Simonov Yu. A., 2005, *Phys. Lett. B*, 619, 293
- Simonov Yu. A., 2008, *Ann. Phys.*, 323, 783
- Simonov Yu. A., Trusov, M. A., 2007, *JETP Lett.* 85, 598
- Simonov Yu. A., Trusov, M. A., 2007, *Phys. Lett. B*, 650, 36
- Smedley S. L., Tout C. A., Ferrario L., Wickramasinghe D. T., 2014, *MNRAS*, 437, 2217
- Sotani H., Yasutake N., Maruyama T., Tatsumi T., 2011, *Phys. Rev. D*, 83, 024014
- Steiner A. W., Lattimer J. M., Brown E. F., 2010, *ApJ*, 722, 33
- Steiner A. W., Lattimer J. M., Brown E. F., 2013, *ApJ*, 765, L5
- Stejner M., Madsen J., 2006, *A&A*, 458, 523
- Stejner M., Madsen J., 2005, *Phys. Rev. D*, 72, 123005
- Suleimanov V., Poutanen J., Revnivtsev M., Werner K., 2011, *ApJ*, 742, 122
- Suleimanov V., Poutanen J., Werner K., 2011, *A&A*, 527, 139

- Thampan A. V., Datta B., 1998, MNRAS, 297, 570
Tomasetti N., 2015, Nucl. Part. Phys. Proc. 265-266, 245
Watts A. L., 2012, ARA&A, 50, 609
Weber F. 2005, Progr. Part. Nucl. Phys., 54, 193
Weissenborn S., Sagert I., Pagliara G., Hempel M., Schaffner-Bielich J., 2011, ApJ, 740, L14
Witten E., 1984, Phys. Rev. D, 30, 272
Xu R. X., Qiao G. J., Bing Z., 1999, ApJ, 522, L109
Xu R.X., Zhang B., Qiao G.J, 2001, Astropart. Phys., 15, 101

APPENDIX A:

It is known (e.g. [Bombaci \(1999\)](#); [Haensel et al. \(2007\)](#)) that the mass and the radius for non-spinning strange stars, in the case of the EOS given in Eq. (9), scale with $B_{\text{eff}}^{-1/2}$. In fact, considering the dimensionless variables:

$$\tilde{P} = P/B_{\text{eff}}, \quad \tilde{\rho} = c^2 \rho / B_{\text{eff}} \equiv \varepsilon / B_{\text{eff}}, \quad (\text{A1})$$

$$\tilde{r} = r/r_o, \quad \tilde{m} = m/m_o, \quad (\text{A2})$$

with

$$r_o \equiv \frac{c^2}{G^{1/2} B_{\text{eff}}^{1/2}}, \quad m_o \equiv \frac{c^4}{G^{3/2} B_{\text{eff}}^{1/2}}, \quad (\text{A3})$$

one can easily show that the TOV equations can be written in the following dimensionless form:

$$\frac{d\tilde{P}}{d\tilde{r}} = -\frac{\tilde{m}\tilde{\rho}}{\tilde{r}^2} \frac{(1 + \frac{\tilde{P}}{\tilde{\rho}})(1 + \frac{4\pi\tilde{r}^3\tilde{P}}{\tilde{m}})}{(1 - \frac{2\tilde{m}}{\tilde{r}})}, \quad (\text{A4})$$

$$\frac{d\tilde{m}}{d\tilde{r}} = 4\pi\tilde{r}^2\tilde{\rho}, \quad (\text{A5})$$

to be solved for any given value of the central density $\tilde{\rho}_c = \tilde{\rho}(0)$ with the boundary conditions $\tilde{m}(0) = 0$ and $\tilde{P}(\tilde{R}) = 0$. Once these dimensionless TOV equations are integrated, the mass and radius of the strange star, for an arbitrary value of the constant B_{eff} , can be obtained from the ‘‘mass’’ \tilde{M} and ‘‘radius’’ \tilde{R} using (A1)–(A3):

$$M_G(\rho_c; B_{\text{eff}}) = \frac{c^4}{G^{3/2} B_{\text{eff}}^{1/2}} \tilde{M}(\tilde{\rho}_c), \quad (\text{A6})$$

$$R(\rho_c; B_{\text{eff}}) = \frac{c^2}{G^{1/2} B_{\text{eff}}^{1/2}} \tilde{R}(\tilde{\rho}_c), \quad (\text{A7})$$

with the central density ρ_c related to the parameter $\tilde{\rho}_c$ by the second of (A1). From equations A6 and A7 one has:

$$M_G(\rho_{c,1}; B_{\text{eff},1}) = \left(\frac{B_{\text{eff},2}}{B_{\text{eff},1}}\right)^{1/2} M_G(\rho_{c,2}; B_{\text{eff},2}), \quad (\text{A8})$$

$$R(\rho_{c,1}; B_{\text{eff},1}) = \left(\frac{B_{\text{eff},2}}{B_{\text{eff},1}}\right)^{1/2} R(\rho_{c,2}; B_{\text{eff},2}), \quad (\text{A9})$$

where $B_{\text{eff},1}$ and $B_{\text{eff},2}$ are two different values of the effective bag constant, and

$$\rho_{c,1}/\rho_{c,2} = B_{\text{eff},1}/B_{\text{eff},2}. \quad (\text{A10})$$

Equations (A6)–(A9) give the scaling law for the mass-radius relation. In particular they hold ([Witten 1984](#); [Haensel et al. 1986](#)) for the maximum mass configuration. Finally, the scaling laws (A8)–(A9) can be extended to the case of spinning configurations. In this case, the stellar structure equations can be written in a dimensionless form ([Haensel et al. 2007](#)) if one supplements the dimensionless quantities (A1)–(A3) with dimensionless angular speeds

$$\tilde{\Omega} \equiv \frac{c}{G^{1/2} B_{\text{eff}}^{1/2}} \Omega, \quad \tilde{\omega} \equiv \frac{c}{G^{1/2} B_{\text{eff}}^{1/2}} \omega. \quad (\text{A11})$$

Thus, the stellar properties for spinning configurations, in the case of the EOS given in Eq. (9), scale with equations (A8)–(A10) supplemented with the following scaling

law for the spin frequency

$$\nu_1 = \left(\frac{B_{\text{eff},1}}{B_{\text{eff},2}}\right)^{1/2} \nu_2. \quad (\text{A12})$$

This paper has been typeset from a $\text{\TeX}/\text{\LaTeX}$ file prepared by the author.

Table 1. Equation of state model parameters used in the present work.

EoS	$B_{\text{eff}}^{1/4}$ (MeV)	a_4
1	138	0.80
2	138	0.61
3	125	0.50

Table 2. Stable structure parameters for the nonspinning maximum mass configurations of strange stars (§ 4).

EoS ¹	ρ_c ²	M_G ³	M_0 ⁴	R ⁵	R/r_g ⁶	r_{orb} ⁷
1	17.682	2.093	2.719	11.559	3.741	18.521
2	17.940	2.073	2.502	11.474	3.749	18.350
3	12.553	2.479	3.090	13.736	3.753	21.893

¹Equation of state models (§ 2 and Fig. 1). ²Central density (10^{14} g cm⁻³). ³Gravitational mass (M_\odot). ⁴Rest mass (M_\odot). ⁵Radius (km). ⁶Inverse of stellar compactness. Here, r_g is the Schwarzschild radius. ⁷Radius (km) of the innermost stable circular orbit, or the stellar equatorial radius, whichever is bigger.

Table 3. Stable structure parameters for the maximally spinning (i.e., mass-shed limit) maximum mass configurations of strange stars (§ 4).

EoS ¹	ρ_c ²	M_G ³	M_0 ⁴	R ⁵	R/r_g ⁶	R_p ⁷	r_{orb} ⁸	J ⁹	ν ¹⁰	I ¹¹	T/W ¹²	Z_p ¹³	Z_f ¹⁴	Z_b ¹⁵
1	11.364	3.032	3.924	17.644	3.942	9.718	19.458	7.080	1412.6	7.973	0.207	0.802	-0.356	2.555
2	11.297	3.001	3.609	17.575	3.967	9.645	19.372	6.963	1415.9	7.827	0.208	0.794	-0.355	2.525
3	7.635	3.600	4.452	21.165	3.983	11.552	23.310	9.940	1170.9	13.505	0.212	0.780	-0.354	2.474

¹Equation of state models (§ 2 and Fig. 1). ²Central density (10^{14} g cm⁻³). ³Gravitational mass (M_\odot). ⁴Rest mass (M_\odot). ⁵Equatorial radius (km). ⁶Inverse of stellar compactness. Here, r_g is the Schwarzschild radius. ⁷Polar radius (km). ⁸Radius (km) of the innermost stable circular orbit, or the stellar equatorial radius, whichever is bigger. ⁹Total angular momentum (10^{49} g cm² s⁻¹). ¹⁰Spin frequency (Hz). ¹¹Moment of inertia (10^{45} g cm²). ¹²Ratio of the total spinning kinetic energy to the total gravitational energy. ¹³Polar redshift. ¹⁴Forward redshift. ¹⁵Backward redshift.

Table 4. Stable structure parameters for the maximum angular momentum configurations of strange stars (§ 4).

EoS ¹	ρ_c	M_G	M_0	R	R/r_g	R_p	r_{orb}	J	ν	I	T/W	Z_p	Z_f	Z_b
1	9.784	3.020	3.892	18.081	4.056	9.670	19.922	7.173	1368.9	8.340	0.215	0.764	-0.353	2.426
2	9.372	2.970	3.550	18.110	4.130	9.567	19.939	7.010	1359.0	8.209	0.216	0.742	-0.351	2.346
3	6.891	3.583	4.415	21.519	4.068	11.504	23.684	9.979	1145.3	13.867	0.217	0.752	-0.352	2.377

¹See Table 3 for meanings of all parameter symbols and units.

Table 5. Three stable configurations on the rest mass ($M_0 = 2.00M_\odot$) sequence for two EoS models.

No. ¹	ρ_c ²	EoS	M_G	R	R/r_g	R_p	r_{orb}	J	ν	I	T/W	Z_p	Z_f	Z_b
1	5.176	1	1.645	14.671	6.039	8.638	16.187	2.104	1063.3	3.149	0.169	0.325	-0.179	0.909
		2	1.768	15.674	6.004	8.228	17.522	2.675	1112.3	3.827	0.201	0.354	-0.219	1.032
2	6.190	1	1.613	12.610	5.297	10.683	12.988	1.099	746.1	2.344	0.058	0.307	-0.008	0.652
		2	1.734	13.441	5.251	10.012	14.554	1.706	949.2	2.861	0.101	0.344	-0.091	0.842
3	6.866	1	1.600	11.822	5.004	11.803	13.675	0.139	108.5	2.045	0.001	0.291	0.246	0.336
		2	1.717	12.572	4.959	10.947	13.410	1.132	719.0	2.505	0.049	0.332	0.018	0.678

¹Number of a specific (M_0, ρ_c) combination. These numbers are marked on the $M_0 = 2.00M_\odot$ sequence in Figs. 3–8. ²See Table 3 for meanings of all parameter symbols and units.

Table 6. Stable structure parameters for the gravitational mass $M_G = 1.97 M_\odot$ and spin frequency $\nu = 317.5$ Hz (measured for PSR J1614-2230) configurations of strange stars (§ 4).

EoS ¹	ρ_c	M_0	R	R/r_g	R_p	r_{orb}	J	I	T/W	Z_p	Z_f	Z_b
1	9.809	2.531	12.165	4.182	11.947	16.012	0.550	2.753	0.007	0.391	0.238	0.551
2	10.309	2.355	12.062	4.147	11.854	16.038	0.540	2.707	0.007	0.396	0.244	0.556
3	4.913	2.362	14.324	4.925	13.872	15.690	0.739	3.702	0.013	0.304	0.147	0.470

¹See Table 3 for meanings of all parameter symbols and units.

Table 7. Stable structure parameters for the constant $\nu = 716$ Hz (measured for the fastest known pulsar PSR J1748-2446ad) sequence of strange stars (§ 4).

EoS ¹	ρ_c	M_G	M_0	R	R/r_g	R_p	r_{orb}	J	I	T/W	Z_p	Z_f	Z_b	
1	3.860	0.197	0.220	6.921	23.829	5.229	6.921	0.035	0.077	0.082	0.053	-0.061	0.168	
	5.045	1.147	1.374	11.648	6.880	9.636	11.648	0.619	1.376	0.061	0.215	-0.032	0.477	
	6.230	1.607	1.989	12.521	5.278	10.777	12.812	1.037	2.305	0.052	0.304	0.004	0.633	
	7.415	1.850	2.334	12.746	4.666	11.227	14.288	1.260	2.800	0.047	0.362	0.032	0.729	
	8.599	1.989	2.537	12.760	4.346	11.401	15.097	1.371	3.047	0.042	0.401	0.054	0.793	
	9.784	2.072	2.663	12.691	4.149	11.473	15.596	1.421	3.157	0.039	0.430	0.071	0.838	
	10.969	2.123	2.742	12.589	4.017	11.461	15.919	1.437	3.193	0.037	0.452	0.086	0.870	
	12.154	2.153	2.790	12.474	3.925	11.433	16.129	1.434	3.185	0.035	0.468	0.098	0.893	
	13.338	2.171	2.819	12.356	3.855	11.377	16.260	1.419	3.152	0.033	0.482	0.108	0.910	
	14.523	2.180	2.835	12.237	3.802	11.336	16.336	1.396	3.103	0.031	0.492	0.117	0.923	
	16.103 ²	2.184	2.842	12.089	3.750	11.242	16.388	1.363	3.029	0.029	0.503	0.127	0.935	
	17.287	2.182	2.840	11.983	3.720	11.170	16.398	1.336	2.969	0.028	0.509	0.134	0.941	
	2	3.950	0.255	0.267	7.491	19.896	5.719	7.491	0.053	0.118	0.076	0.064	-0.062	0.191
		5.108	1.128	1.257	11.542	6.928	9.589	11.542	0.598	1.328	0.060	0.213	-0.031	0.472
6.265		1.574	1.809	12.404	5.338	10.678	12.404	0.996	2.212	0.052	0.300	0.004	0.622	
7.423		1.815	2.124	12.635	4.716	11.133	14.061	1.212	2.693	0.046	0.356	0.031	0.717	
8.581		1.954	2.314	12.662	4.389	11.314	14.878	1.324	2.942	0.042	0.395	0.053	0.780	
9.739		2.040	2.434	12.601	4.185	11.393	15.386	1.378	3.060	0.039	0.424	0.070	0.825	
12.054		2.125	2.557	12.402	3.954	11.365	15.947	1.397	3.104	0.034	0.463	0.097	0.881	
14.369		2.156	2.604	12.176	3.826	11.278	16.175	1.366	3.035	0.031	0.487	0.116	0.912	
16.299 ²		2.161	2.614	11.998	3.760	11.164	16.249	1.328	2.951	0.029	0.500	0.128	0.927	
17.456		2.160	2.612	11.896	3.731	11.096	16.258	1.302	2.894	0.028	0.506	0.135	0.933	
3		2.920	0.700	0.765	12.181	11.793	8.216	12.181	0.388	0.862	0.134	0.123	-0.100	0.353
	3.913	1.764	2.057	15.246	5.856	11.798	15.575	1.647	3.660	0.089	0.281	-0.067	0.664	
	5.154	2.275	2.746	15.699	4.673	12.938	17.538	2.332	5.181	0.071	0.379	-0.028	0.845	
	6.147	2.457	3.006	15.618	4.306	13.239	18.290	2.522	5.603	0.063	0.425	-0.004	0.925	
	7.139	2.552	3.149	15.443	4.099	13.348	18.725	2.578	5.727	0.057	0.457	0.015	0.975	
	8.132	2.603	3.229	15.244	3.966	13.345	18.980	2.571	5.712	0.052	0.479	0.031	1.008	
	9.125	2.629	3.271	15.043	3.876	13.317	19.118	2.529	5.619	0.049	0.495	0.044	1.030	
	10.118	2.639	3.290	14.852	3.812	13.239	19.189	2.474	5.497	0.046	0.507	0.054	1.045	
	10.863 ²	2.640	3.294	14.714	3.774	13.188	19.204	2.427	5.393	0.044	0.515	0.061	1.052	
	12.352	2.633	3.287	14.460	3.720	13.056	19.186	2.331	5.180	0.041	0.525	0.073	1.062	

¹See Table 3 for meanings of all parameter symbols and units. ²Maximum mass configurations for $\nu = 716$ Hz, and for chosen EoS models.